Alkali activation of bottom ash from municipal solid waste incineration:

Optimization of NaOH- and Na$_2$SiO$_3$-based activators

R. Carvalho[1], R. V. Silva[1*], J. de Brito[1], M. F. C. Pereira[2]

1 CERIS, Instituto Superior Técnico, Universidade de Lisboa, Av. Rovisco Pais, 1049-001 Lisboa, Portugal
2 CERENA, Instituto Superior Técnico, Universidade de Lisboa, Av. Rovisco Pais, 1049-001 Lisboa, Portugal
*Corresponding author e-mail: rui.v.silva@tecnico.ulisboa.pt; Other e-mails: ricardo_carvalho_@msn.com; jb@civil.ist.utl.pt; mfcp@ist.utl.pt

Abstract: Considerable amounts of municipal solid waste incinerator bottom ashes are produced yearly without an adequate outlet. Given the established reactivity of the ash when subjected to an alkali medium, there is considerable scope to valorize it within the Construction industry in an alkali-activated material, thereby reducing the significant environmental pressure of the cement industry. This study assesses the optimization of alkali-activated mortars, using milled municipal solid waste incinerator bottom ash as a precursor, from mechanical and durability behaviour perspectives, many properties of which have never been analysed. The alkaline solution is comprised of either NaOH or Na$_2$SiO$_3$ (Na$_2$O/precursor ratio varying between 9.1% and 24.2% and SiO$_2$/Na$_2$O ratios of 0 or 1.0); fly ash from a coal-fired power plant was also used as control precursor. X-ray fluorescence and powder X-ray diffraction analyses of cement, fly ash, bottom ash and of the resulting pastes were carried out. All specimens were evaluated in terms of their mechanical and durability-related performance (i.e. flexural and compressive strength, carbonation, water absorption by capillary action, and shrinkage). Considerable generation of H$_2$ gas was observed during production, resulting from the reaction between the bottom ashes' metallic aluminium fraction and the NaOH solution, leading to significant expansion and an overall increase in porosity and thus a strong decline in performance. Alkali-activated bottom ash specimens presented fast carbonation, resulting in a considerable strength increase. Despite the low performance of most of these mixes, the strength enhancement of specimens subjected to some conditions infers that there is significant scope for further mix design optimization (e.g. aluminium reduction, mixing time, Na$_2$O/precursor and SiO$_2$/Na$_2$O ratios) that can lead to the manufacture of fit-for-industry construction materials.

Keywords: mortar; municipal solid waste; incinerator bottom ash; alkali-activated materials; NaOH; Na$_2$SiO$_3$.

Declarations of interest: none

Notation list

AAM - alkali-activated material

EDS - energy-dispersive X-ray spectroscopy

FA - fly ash

GGBS - ground granulated blast furnace slag

MIBA - municipal solid waste incinerator bottom ashes

MSW - municipal solid waste

PC - Portland cement

SEM - scanning electron microscopy

XRD - X-ray diffraction

XRF - X-ray fluorescence

1 Introduction

The cement industry contributes around 5-7% of the total global CO_2 emissions (Benhelal et al., 2013), thereby making it of fundamental importance to seek new solutions that can further decrease its environmental impact. One of the most recently developed alternatives to cement is the use of aluminosilicate by-products from several industrial processes as precursors in alkali-activated materials (AAM). These materials, which result from the dissolution of amorphous silica and alumina phases present in natural/industrial waste resources, can exhibit considerable mechanical and durability performance. These binders can immobilize heavy metals in their crystalline structure, present high resistance to acid attack, present fast setting at room temperature, and high compressive strength (Davidovits, 1994). Additionally, the production of AAM was found to present less 55-75% CO_2 emissions in comparison with cement-based materials (Yang et al., 2013), thereby making them a technically viable and environmentally friendly alternative to cement.

Fly ash (FA) and ground granulated blast-furnace slag (GGBS) are typical by-products of AAM production. A considerable amount of research has been carried on these two precursors and there have been some applications within the Construction sector (Provis and van Deventer, 2014). Nevertheless, given the Energy Industry's generalized shifting towards renewable sources, the production of FA has been decreasing thus affecting the future supply chain for FA-based AAM. Also, electric arc furnaces have been preferred over blast furnaces due to their higher efficiency for recycling ferrous metals, thereby decreasing the production of GGBS. Since the slag from the former furnace is likely to present lesser reactivity potential in comparison with the latter furnace's slag (Ozturk et al., 2019), the study of other aluminosilicate by-products is necessary for AAM production.

In 2012, the total global production of waste amounted to about 1.3 billion tonnes and, in 2025, this value is expected to reach up to 2.2 billion tonnes, representing 1.42 kg/person/day (Silva et al., 2017). One of the most effective measures to treat municipal solid waste (MSW) is using incineration with energy recovery, which is capable of reducing the initial weight by around 75% (Dhir et al., 2018). However, this industry is responsible for two by-products: MSW incinerated fly ashes and bottom ashes (MIBA). In Lisbon, Portugal, about 100 kt/y of MIBA (85-95% of the incinerated product), come from Valorsul's incineration unit treating most of the city's MSW. The resulting MIBA is then processed to be used in construction, but

most of it is left unused in sanitary landfills.

MIBA has been successfully used in the production of AAM but is still in it its early stages of research. Most publications on the matter are recent and have focused mostly on understanding the most adequate concentration of the alkaline activator (AA) to enhance the performance. Chen et al. (2016) produced aerated MIBA-based AAM. The concentrations of the NaOH solutions were 2 M, 4 M, 8 M and 12 M and mix duration ranged from 15 to 120 min to potentiate metallic Al corrosion and thus H_2 gas production. A concentration of 8 M and mixing for 60 min were found to be optimum in terms of compressive strength (maximum compressive strength of 2.82 MPa) and porosity. Further increasing mixing time resulted in enhanced performance due to H_2 release rather than leaving it entrapped in the fresh mix.

Zhu *et al.* (2018) studied the characteristics of AAM using the glass fraction collected from MIBA using different contents of the AA. Aqueous Na_2SiO_3 and NaOH were used as activators in mixes with an l/s ratio of 0.5 and subsequently cured at 75 °C and 98% RH for 3 days. The 3-day compressive strength of the samples with MIBA was around 3 MPa, whereas specimens made with the glass fraction alone presented compressive strengths close to 70 MPa. This increase was due to the use of milled glass only, which increased the amount of amorphous material capable of reacting with the alkaline solution (Golek, 2019). Increasing the SiO_2/Na_2O ratio of the alkaline solution from 0 to 2.5, to understand the optimum levels of the activator, led to a near 60 MPa increase in compressive strength with the specimens exhibiting considerable nano-structural connectivity from increased polymerization degree of the gel (Zhu et al., 2019).

Kim and Kang (2014) focused on optimizing the l/s ratio, NaOH concentration, and particle size of vitrified MIBA in alkali-activated specimens. For a fixed particle size of 45 μm of the highly amorphous vitrified MIBA, increasing the NaOH concentration from 14 M to 25 M led to an increase in 1-day compressive strength of ~40 MPa to ~160 MPa, respectively, wherein stabilization occurred after 20 M concentration (optimum concentration). Similar high strength was achieved recently in a study attempting to recreate the vitreous fraction of the product of MSW incineration via a high-temperature vitrification process (Ascensão et al., 2020). Mixes with solid to liquid ratios of 2.5, using vitrified MIBA and silica fume, resulted in 28-day compressive strengths of 90-120 MPa, which increased with the use of K_2SiO_3 for the same K_2O/SiO_2 ratio.

Wongsa *et al.* (2017) produced alkali-activated mortars using MIBA and type C FA as precursors. MIBA was ground by ball mill to a maximum particle size of 45 μm. 10 M NaOH and aqueous Na_2SiO_3 solutions were used as activators. Optimum 28-day compressive strength was observed for specimens with 20% MIBA and 80% FA (about 53 MPa), whereas 100% MIBA led to a value of 10.6 MPa. Apart from the clear trend in the pore size distribution results, porosity, compressive strength and SEM, the incorporation at 20% of MIBA with FA was deemed as optimum for use as a precursor in alkali-activated mortars.

Huang *et al.* (2018, 2019) assessed the performance of mortars containing 60% MIBA and 40% GGBS, with special focus on the binder's active components. The compressive strength of the alkali-activated samples without Na_2SiO_3 was relatively low (~15 MPa after 28 days) due to low amorphous SiO_2 content, which affected the nucleation and growth of C-A-S-H and C-S-H. Mechanical performance improved (~50 MPa after 28 days) after incorporating about 26% of liquid Na_2SiO_3 (SiO_2/Na_2O ratio of 1.04). A higher quantity of Na_2SiO_3 hindered the strength development due to excess of activated sodium and silicon, causing the precipitation of magadiite ($NaSi_7O_{13}(OH)_3 \cdot 4(H_2O)$), which is known for its instability and low hardness.

The main objective of this study was to evaluate the performance of alkali-activated mortars with MIBA as the precursor, in an attempt to further valorize the by-product, thereby reducing its landfilling and preventing the excessive use of cement as a binding material (Silva et al., 2017). This study is one of the firsts in a state-funded research project in Portugal, involving companies within the construction sector, aiming to further reduce the environmental impacts and cost associated with the production of structural concrete through the alkali-activation of MIBA as integral replacement of cement. The aforementioned studies dealt, in some manner, with the optimization of the AA to enhance the performance of MIBA-based alkali-activated materials. However, since it is a topic that is still in its early stages of research, there is a considerable gap in the literature before advancing with the standardization or commercialization of the material (Kurda et al., 2020). The literature review demonstrates that attempts have been made to optimize the AA, but few studies have been carried out on the activation of MIBA alone and, based on the highlighted behaviour in previous studies, as well as preliminary results obtained by the authors, there is significant scope for performance enhancement of AAM comprised solely of MIBA. Furthermore, another novelty of this study is the synthesis of the alkaline solution (aqueous Na_2SiO_3)

using anhydrous SiO_2 pellets (no study exists in the literature in combination with MIBA as a precursor), following a "two-part alkali-activated material" approach to further understand its role in potential "one-part alkali-activated materials" (or "just add water") (Luukkonen et al., 2018). Additionally, in contrast with all other studies that have produced activated MIBA-based mixes, the ones presented in this paper underwent a resting period after mixing to potentiate H_2 generation from the corrosion of Al. Finally, not only there is no study in the literature analysing the drying shrinkage behaviour of alkali-activated MIBA-based mixes, but there is also none on the strength development of such mixes when subjected to an accelerated carbonation curing. The behaviour of some of these mortars is compared with that of cement mortars and alkali-activated mortars with FA as a precursor. X-ray fluorescence (XRF) and powder XRD analyses were carried out on cement, FA, MIBA and selected mortars. The specimens' mechanical and durability-related performances were evaluated through their flexural and compressive strength, carbonation, water absorption by capillary action, and shrinkage.

2 Materials and methods

2.1 Mix design

The mortars' mix design followed a method proposed in another study (Nepomuceno et al., 2012), which yields mortars exhibiting characteristics and performance equivalent to those of a concrete counterpart and not mortars typically used in for rendering and masonry. All mortars had a volumetric proportion binder/aggregates of 1/3 (equivalent to 564 g and 1700 g, respectively) and a liquid/binder ratio by mass of 0.5 to compare mortars made with cement, FA and MIBA, and 0.65 to analyse MIBA mortars with a variation of the AA.

Table 1 - Identification of the alkaline activator for mortar production

| Binder | NaOH (mol/kg) | M_{NaOH}/M_{H2O} (%) | M_{Na2O}/M_{binder} (%) | Percentage by mass (%) | | | Designation |
				H_2O	Na_2O	SiO_2	
MIBA	4.5	18.0	5.29	78.2	10.9	10.9	NS1
	5.6	22.5	6.24	74.1	12.9	12.9	NS2
	6.8	27.0	7.08	70.5	14.8	14.8	NS3
	8.0	32.0	12.4	80.1	19.9	0.0	N1
	10.0	40.0	15.5	76.3	23.7	0.0	N2
	12.0	48.0	18.6	72.9	27.1	0.0	N3
FA	10.0	40.0	15.5	76.3	23.7	0.0	FA
Cement	0.0	0.0	0.0	100.0	0.0	0.0	CEM

The experimental campaign was organized in four phases: in the first one, the properties of the materials were determined (i.e. cement, FA, MIBA, aggregates); in the second phase, experimental mixes were produced to determine the best mixing and curing processes of MIBA mortars (workability and flexural and compressive strength tests); in phase three, cement, FA and MIBA mortars were compared with liquid/binder ratio of 0.5; in the last phase, only MIBA was used as binder and AA varied, with AA/MIBA ratio of 0.65 to obtain a target slump of 175 ± 15 mm. All AAM samples were cured at 70 °C for 24 h and subsequently placed in a controlled chamber at 20 ± 3 °C with a relative humidity of 50% until their testing age.

2.2 Material characterization

Cement CEM I 42.5R (PC) was used as the control for conventional mortars. Class F coal FA (ASTM C618, 2015), provided by the Portuguese cement producer Secil, was used as the control binder for AAM. MIBA was sourced from the Valorsul's MSW treatment plant, located in São João da Talha, in the municipality of Loures, Portugal. For PC and MIBA, the XRF was analysed with the use of a Niton XL3T GOLDD spectrometer with an X-ray generator of 50 kV/200 μA, equipped with a CCD for image location (3 mm spot diameter) and storage, whereas the composition of FA was obtained by wavelength dispersive XRF, using an S4 Pioneer apparatus of BRUKER, with a potential of 4 kV. Additionally, for the characterization of MIBA, scanning electron microscopy (SEM), and energy-dispersive X-ray spectroscopy (EDS) were carried out. XRD analyses were also performed in all binders using a Bruker D8 Discover A25 instrument with Cu-Kα radiation. Diffraction patterns were obtained by scanning the goniometer from 10° to 80° (2θ) at a rate of $0.05°·s^{-1}$. The pozzolanicity of MIBA and FA was quantified using the Chapelle test (Ferraz et al., 2015; NBR-15895, 2010), through which the consumption of calcium oxide (CaO) per gram of by-product (MIBA and FA) was determined.

MIBA was also subjected to a test quantifying the portion of metallic Al through its reaction with aqueous NaOH. An 800 ml solution of 2.5 M NaOH was placed in a three-nozzle balloon along with 10 g of MIBA, or 0.1 g of Al powder as control, and connected through a glass tubing to an inverted test tube to measure displaced volume. Three runs were performed, each of which for a period of 24 h. Equation 1 shows the chemical reaction behind this process and, in terms of the stoichiometric quantities (atomic and molecular weights).

$$2Al + 2NaOH + 6H_2O \rightarrow 2NaAl(OH)_4 + 3\,H_2 \uparrow \tag{1}$$
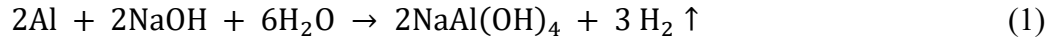
Through the stoichiometry of reaction 1, the measured volume of released H2 allowed calculating the content in grams of metallic Al present in MIBA, after proper comparison with a control test using pure Al powder.

The water used in the production of all specimens was potable tap water. For mortars with MIBA, a ligno-sulphonate-based water-reducing admixture was used (2% of Sikament 400 Plus by weight of binder). The AA was a solution of either NaOH (99% purity) or Na_2SiO_3 (solution containing NaOH and solid SiO_2 pellets). The fine aggregates were composed of fine and coarse siliceous sand (with particle size distributions ranging from 0 to 1 mm and 0 to 4 mm, respectively). The sand's particle size distribution was made following EN 1015-1 (1999). The bulk density was evaluated according to EN 1097-3 (1998), whereas water absorption and apparent densities as per EN 1097-6 (2008).

2.3   Testing methods of mortar specimens

Mortars were produced and cast following EN 1015-2 (1999) with some variations given the necessity of thermal curing. The consistence of fresh mortars was tested following EN 1015-3 (1999), bulk density with EN 1015-6 (1999), dynamic Young's modulus with ASTM E1876 (2015), flexural and compressive strength with EN 1015-11 (1999), carbonation (28 to 91 days in a carbonation chamber at 23 ± 3 °C, $60 \pm 5\%$ relative humidity and a CO_2 concentration of $5.0 \pm 0.1\%$) with LNEC E391 (1993), water absorption by capillary action with EN 1015-18 (2002), and shrinkage with EN 1015-13 (1993). MIBA and selected pastes thereof were analysed through XRD.

3   Results and discussion

3.1   Material characterization

Table 2 presents the composition of the main oxides of PC, MIBA and FA. The composition of FA is as expected from a Class F; the sum of $Al_2O_3 + SiO_2 + Fe_2O_3$ is equal to 84.8% and exceeds the minimum value established (i.e. 70% by weight) as per EN 450-1 (2012). The composition of MIBA shows lower content of Al_2O_3 and Fe_2O_3 and a considerably larger fraction of CaO. According to ASTM C618, MIBA could be classified as class C FA, wherein the minimum value of the sum of Al_2O_3, SiO_2 and Fe_2O_3 is 50 wt%.

Table 2 - X-ray fluorescence of PC, FA and MIBA

Material	SiO$_2$ (%)	Al$_2$O$_3$ (%)	Fe$_2$O$_3$ (%)	CaO (%)	MgO (%)	SO$_3$ (%)	K$_2$O (%)	TiO$_2$ (%)	CuO (%)	Na$_2$O (%)	P$_2$O$_5$ (%)
PC	19.49	5.02	3.32	63.48	1.26	3.26	-	-	-	-	-
FA	51.93	18.75	15.96	4.46	0.90	-	3.24	2.39	1.60	0.76	-
MIBA	51.84	5.00	9.29	23.00	2.36	2.42	1.57	0.34	0.16	-	2.29

The accumulated particle size distribution of MIBA, by hand wet sieving, after a ball mill processing are the following: 93.1% passing the 106 μm sieve; 58.1%, the 53 μm; 52.6%, the 45 μm; and 39.3%, the 23 μm. The average particle size of MIBA is just under 45 μm. The XRD analysis (**Error! Reference source not found.**) showed that MIBA contains a significant amorphous fraction (broad reflexion peak between the 15º and 40º 2θ positions), which can be mostly attributed to the waste glass fraction. This was confirmed by stereomicroscope observations using an Olympus SZ51 stereomicroscope (**Error! Reference source not found.**).
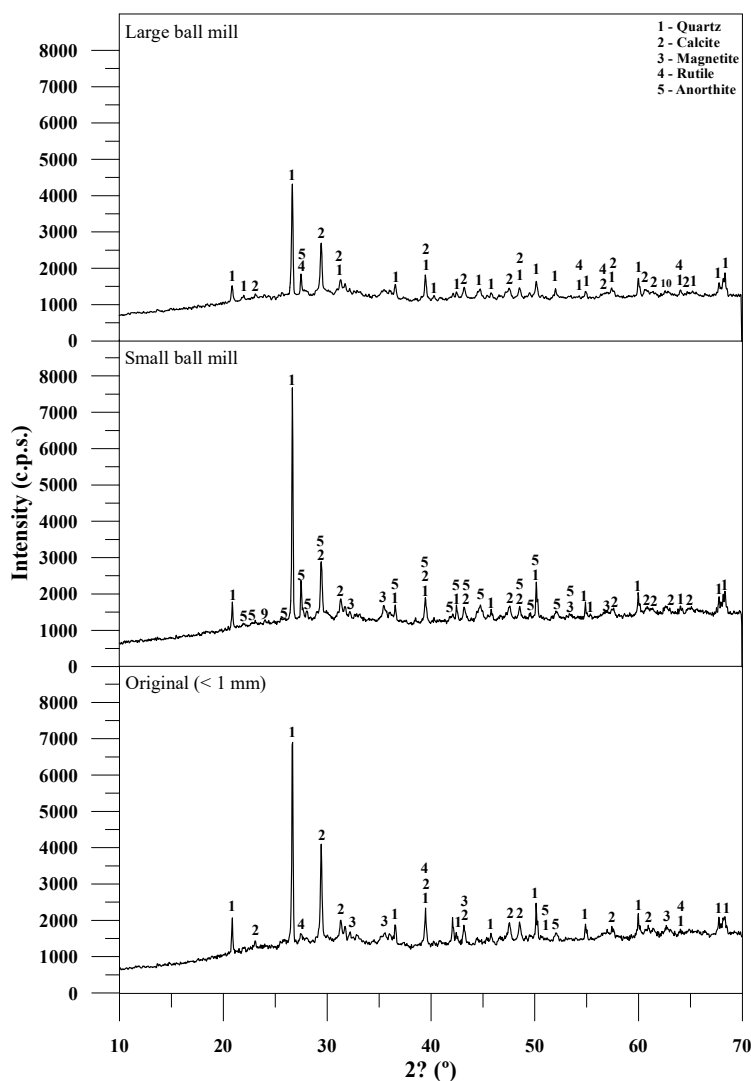
Figure 1 - XRD of MIBA processed in the large and small ball mills and original material under 1 mm

Figure 2 - Stereomicroscopic image of a sample of washed MIBA (G - glass with different colours; C - different kinds of ceramic; S - siliceous sand particles; Cu - copper-based metallic agglomerate, also containing iron and aluminium)

Samples coming from different procedures were analysed in terms of XRD to understand the effect of the process on the mineralogy of the materials (unprocessed MIBA; processed in a small ball mill with a capacity of 1 kg; and processed in a large ball mill with a capacity of 20 kg). As expected, similar profiles were obtained, but a decrease in quartz peaks (SiO_2 - International Centre for Diffraction Data - ICDD # 33-1161) was observed in MIBA processed in the large ball mill. Quartz crystallinity has been reduced along with size, which could improve its reactivity. Other mineralogical phases included calcite ($CaCO_3$ - ICDD # 05-0586), kamacite (Fe, Ni - ICDD # 37-0474) and magnetite (Fe_3O_4 - ICDD # 03-0863).

After performing a magnetic separation stage, using a neodymium magnet, of a 24-g random sample of MIBA, the results showed that 11.6% and 89.4% corresponded to magnetic and non-magnetic phases, respectively, thus demonstrating that the electromagnetic separation stage applied at the MIBA's treatment facility was not optimized and further quantities of material could be recovered. Phase separated XRD analysis showed main peaks of quartz (SiO_2 - ICDD # 33-1161), calcite ($CaCO_3$ - ICDD # 05-0586) and anorthite ([Ca, Na][Si, Al]$_4O_8$ - ICDD # 20-0020) for non-magnetic fraction and, for the magnetic fraction, magnetite (Fe_3O_4 - ICDD # 03-0863) and kamacite (Fe, Ni - ICDD # 37-0474).

Figure 3 presents the morphology of MIBA. Most of the particles have an angular shape and according to previous studies, these are likely to present a porous microstructure and thus it is probable that a greater amount of water is needed to cover their surface area for given workability (Silva et al., 2017; Tang, 2017). The results of

the EDS test showed that the elemental composition of fine fractions of MIBA corresponded to around 23.3%

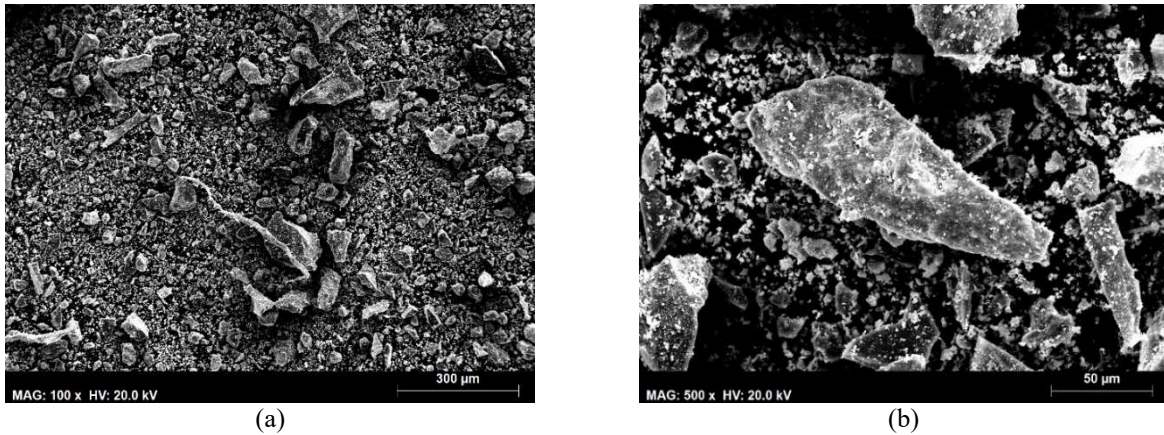for oxygen, followed by calcium with 15.2%, 8.7% for silicon, 6.63% of aluminium and 4.1% of iron.

<div align="center">(a)   (b)</div>

<div align="center">Figure 3 - SEM of MIBA</div>

Modified Chapelle test determined, by titration with 0.1 M HCl, the content of unconsumed free $Ca(OH)_2$

by the reactive phases present in the FA and MIBA during 16 h of reaction at 90 ± 5 °C, using of 2 g CaO

laboratory grade and 1 g of FA/MIBA in distilled water. Reactions 2 and 3 were present in the titration.

$$CaO + 2HCl \rightarrow CaCl_2 + H_2O \tag{2}$$

$$Ca(OH)_2 + 2HCl \rightarrow CaCl_2 + 2H_2O \tag{3}$$
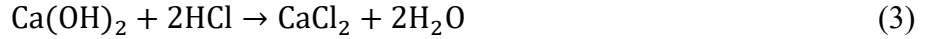
Through equation 4, it is possible to calculate the mg of $Ca(OH)_2$ / g of FA/MIBA (NBR-15895, 2010).

$$\frac{mg\ Ca(OH)_2}{g\ by-product} = \frac{28 \cdot (v_3 - v_2) \cdot F_c}{m_2} \times 1.32 \tag{4}$$

Where, m_2 is the mass of the pozzolanic material expressed in grams, v_2, the volume of HCl consumed by

the sample in ml; v_3, the volume of HCl consumed by the blank in ml; Fc, the correction factor for a 0.1 M

solution; and 1.32 is the molecular relationship between $Ca(OH)_2$ / CaO. Values of 566 mg and 445 mg of

$Ca(OH)_2$ were obtained per g of residue for FA and MIBA, respectively, which are higher than the mini-

mum limit of 436 mg $Ca(OH)_2$ / g of addition, established by Raverdy *et al.* (1980) for the classification of

a pozzolanic mineral addition. Both products can be considered as pozzolanic.

In the quantification of metallic Al, the quantities of each of the reactants and products generated in grams

are presented in equation 5, which corresponds to equation 1. 0.11 g of $H_2\uparrow$ were expected to be produced

per gram of Al consumed. A displaced volume of 131.3 ± 5.0 ml was observed per 0.1 g of Al powder. The temperature of the reaction was 43 °C (exothermic reaction of NaOH in water). The density of H_2 at 43 °C and 1 atm. pressure is 0.0766 kg/m^3. From this property and the mass of H_2 produced per gram of Al, it was possible to determine the theoretical volume of H_2 generated.

$$54\,g \;+\;\; 80\,g \;\; + 108\,g \;\rightarrow\;\; 236\,g \;\;\;\;\; + \; 6\,g \uparrow \tag{5}$$
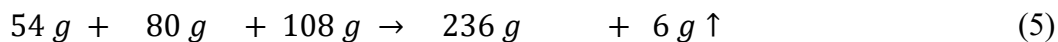
In this test, 10 grams of MIBA reacted with a 2.5M solution of NaOH and released 63.3 ml of H_2, corresponding to 43.65 mg of Al. Therefore, there are around 4.36 g of Al for each kg of MIBA and that 6.3 L of $H_2\uparrow$ are released for each kg of MIBA.

The particle size distribution test of the aggregates showed that the values of D_{max} were 1 mm and 4 mm for fine and coarse sands, respectively, and the fineness moduli 2.37 and 3.62, respectively. The results of apparent (ρ_a), rodded-dry (ρ_{rd}) and saturated and surface-dried (ρ_{ssd}) densities for the two types of sand were: $\rho_a = 2652$ kg/m^3, $\rho_{rd} = 2624$ kg/m^3 and $\rho_{ssd} = 2634$ kg/m^3, for fine sand; $\rho_a = 2636$ kg/m^3, $\rho_{rd} = 2601$ kg/m^3 and $\rho_{ssd} = 2614$ kg/m^3, for coarse sand. In terms of bulk density (ρ_b), the results were 1544 kg/m^3 and 1556 kg/m^3, for fine and coarse sand, respectively. In the water absorption test, the result for fine sand, at 24 h, was $WA_{24} = 0.40\%$ and, for coarse sand, 0.51%.

3.2 Properties of mortars with different binders

3.2.1 Fresh state performance

Mortars produced with PC and alkali-activated FA and MIBA were compared (binder/aggregates of 1/3; liquid/binder of 0.5; Na_2O/binder of 15.5%; and AA composed of 76.3% H_2O and 23.7% Na_2O). For MIBA mortars, 2% of a water-reducing admixture was added during production. PC mortars showed the highest levels of consistence with an average slump flow of 223 mm. FA-based AAM showed lower values of 187 mm due to NaOH in the solution, which increased viscosity (Schalenbach et al., 2018). The slump values MIBA mortars were much lower, with an average slump flow of 107 mm. This can be explained, mainly, by the particles' morphology. MIBA has irregular, angular and flat particles, which resulted in low workability, making it difficult to compact them. The fresh density of MIBA mortars was also lower than that of

the FA and PC mortars (1873 kg/m^3, 2245 kg/m^3 and 2246 kg/m^3, respectively). The lower density is mostly attributed to the porous structure from generated H$_2$ gas.

3.2.2 Hardened state performance

PC and FA specimens showed similar dimensional stability, but the first had higher mass and thus greater density. MIBA and FA specimens presented similar masses. However, due to the formation of H$_2$ (Figure 4a), MIBA specimens increased in volume (Figure 4b), consequently, decreasing bulk density.

| (a) | (b) |

Figure 4 - H$_2$ gas formation in the preparation of mortars (a) and expanded mortar (b)

PC-based specimens showed higher dynamic moduli of elasticity at 7 and 28 days (35 GPa and 37 GPa, respectively). The dynamic modulus of elasticity increased by about 7% for PC, and more than 35% for FA (17 GPa and 23 GPa for 7 and 28 days, respectively). The MIBA family showed the lowest values (10 GPa and 11 GPa for 7 and 28 days, respectively). The highest ultrasonic pulse velocity values were those of PC mortars (4586 m/s, 3537 m/s and 2761 m/s for PC, FA and MIBA mortars, respectively). MIBA specimens, due to the high porosity of the samples, the velocity of the ultrasonic waves was lower and the evolution was only 5%.

The flexural strength of FA and MIBA specimens increased by ~100% between 7 and 28 days, compared to less than 30% for PC mortars. FA mixes showed the highest 28-day values (Figure 5a). FA-based AAM and with different AA may exhibit significantly varying strength in the first 28 days, due to slow polymerization reactions (Olivia and Nikraz, 2012). Lower ultrasonic waves pulse velocities of AAM mixes are likely to be observed, but

better results for flexural strength are more probable, because of its three-dimensional structure as a result of the polymerization reactions providing physical strength. Furthermore, the high content of silicates can also increase the elasticity of AAM (Olivia and Nikraz, 2012). The compressive strength of MIBA specimens showed the same trend as in the flexural test, due to the specimens' high porosity. The poor strength was a result of the generated gas, which significantly increased the specimens' porosity. Furthermore, MIBA contains low content of amorphous silica thus affecting the dissolution, formation and growth polymer chains (Huang et al., 2019).
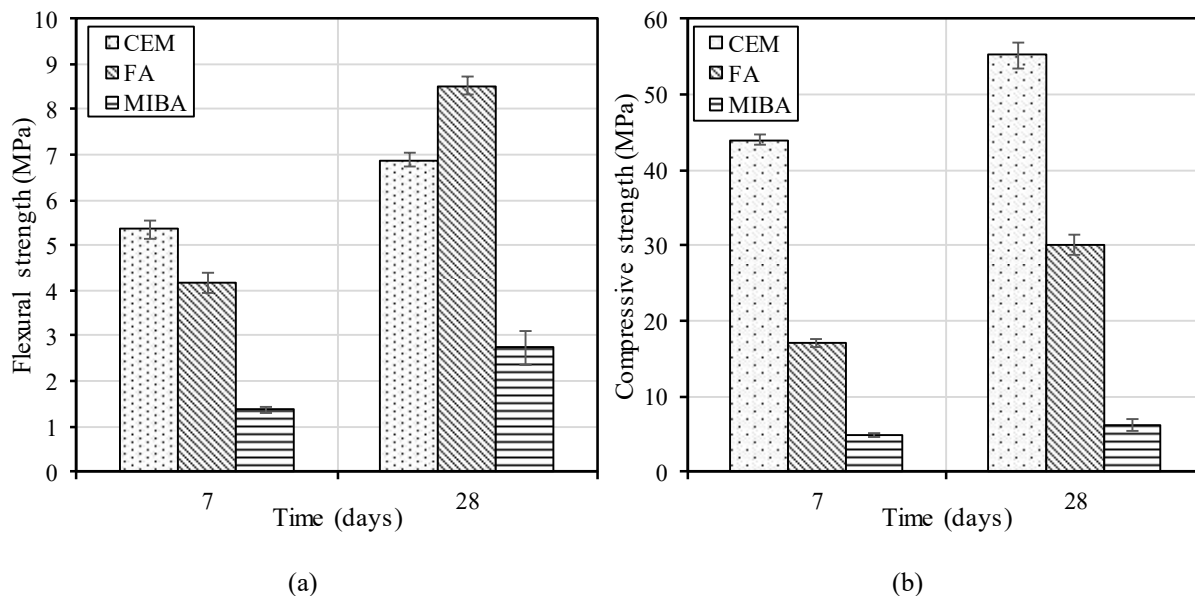
Figure 5 - Flexural strength (a) and compressive strength (b) of PC, FA, and MIBA specimens at 7 and 28 days

3.3   Properties of MIBA mortars with different activators

3.3.1   Fresh state performance

Mortars with NaOH only showed a loss in workability with an increasing amount of solute in the activator and, consequently, the decrease of water content. Since MIBA particles exhibit a high water requirement, together with the decrease in the amount of water and higher viscosity of AA, the slump flow decreased slightly (N1 - 185 mm; N2 - 181 mm; N3 - 173 mm).

The use of Na_2SiO_3 required a change in the mixing process due to the development of accelerated setting and thus no resting period was allowed for the release of H_2 gas. The reduction of the setting time can be explained by the uncontrolled formation of the initial phases of C-S-H gel (Palacios et al., 2008). The results for workability showed a different trend when compared with mixes with only NaOH, improving with the

decrease of water and the increase of NaOH in AA. This may have been due to the execution of the test when the reactions of the MIBA constituents with the AA were still ongoing for the most part. After a mixing process of only 5 minutes, the high amount of H_2 gas still entrapped in the mix may have aided in the mixes' flow (NS1 - 164 mm; NS2 - 186 mm; NS3 - 188 mm).

Bulk density slightly increased with the increase of NaOH in the AA (N1 - 1750 kg/m^3; N2 - 1757 kg/m^3; N3 - 1775 kg/m^3). This was mostly due to the density increase of the liquid with the addition of the constituent. However, for mortars with Na_2SiO_3, the trend is again the opposite (NS1 - 1962 kg/m^3; NS2 - 1876 kg/m^3; NS3 - 1845 kg/m^3). The production of H_2, which has a direct relationship with the NaOH content in AA, led to the formation of more voids and, consequently, affected the mortar's compaction inside the mould.

3.3.2 Hardened state performance

All MIBA-based mixes presented expansion. Mortars made with the NaOH solution exhibited greater increases in volume, the magnitude of which was greater for higher concentrations of NaOH. In mortars with Na_2SiO_3, the expansion was less noticeable, despite the abundant presence of gas in the mix. The fast partial setting of the mortar (Palacios et al., 2008) and lower content of OH^- ions (slower H_2 generation) may have limited the increase of volume. However, the gas release and the strength development occurring simultaneously impaired the mortar's compaction, causing loss of material after the process, affecting the mass of the specimens, which became lighter and more porous.

Apart from the expansion, other problems in mortars with Na_2SiO_3 included adhesion to the mould, resulting in some detachment of material, and efflorescence. The latter phenomenon may have been due to the insufficient growth and binding of solid phases, leading to overall poor strength in the microstructure. XRD analysis (Figure 6) showed that this efflorescence was comprised mostly of trona ($Na_3H(CO_3)_2 \cdot 2H_2O$ - ICDD # 029-1447), thermonatrite ($Na_2CO_3 \cdot H_2O$ - ICDD # 001-1015) and halite (NaCl - ICDD # 001-0994). These results show leaching of Na^+, thus indicating an excessive concentration of NaOH that did not partake in the reaction (Provis and van Deventer, 2014).

The higher concentration of NaOH in the N2 and N3 specimens led to a greater development of the microstructure when compared with N1 specimens. However, the molal concentration of 12 mol/kg (i.e. N3) caused greater internal porosity and, consequently, a decrease in the dynamic modulus of elasticity and ultrasonic pulse velocity (Table 3), when compared with mortars with a concentration of 10 mol/kg (i.e. N2). Mixes with Na_2SiO_3 presented lower results, as the mortars were more porous and efflorescence appeared on the surface, indicating loss of material and lower internal cohesion.
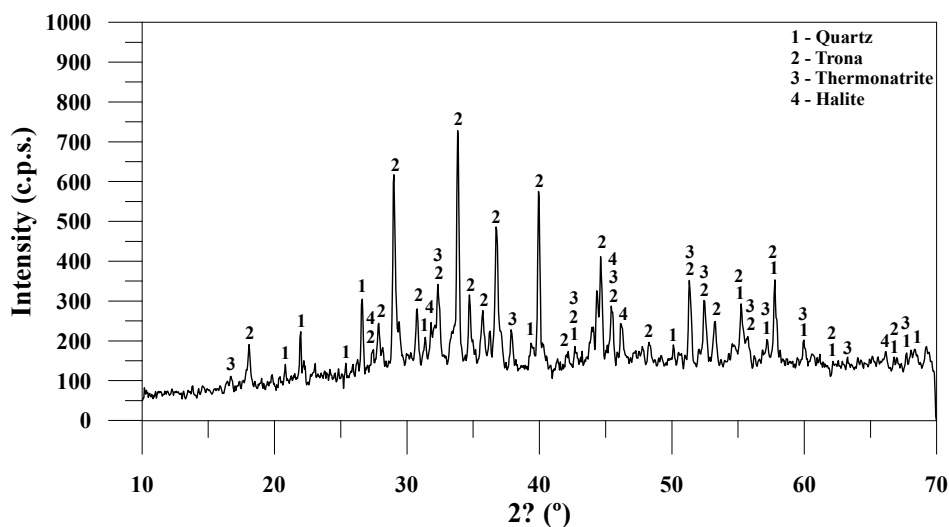
Figure 6 - XRD analysis of efflorescence precipitates

Table 3 - Ultrasonic pulse velocity

Mix	7-day		28-day		91-day	
	$\bar{x}$ (m/s)	s (m/s)	$\bar{x}$ (m/s)	s (m/s)	$\bar{x}$ (m/s)	s (m/s)
N1	2116	12	2425	31	2651	28
N2	2141	15	2633	34	2973	19
N3	2142	40	2515	27	2864	61
NS1	1163	134	-	-	957	2
NS2	1473	33	1389	17	1400	113
NS3	1604	42	1740	29	1837	19

Figure 7 presents the results of the flexural and compressive strengths. The increment of NaOH concentration up to 10 mol/kg (i.e. N2) led to optimum results although comparable compressive strength values were also observed for mixes with 8 mol/kg (i.e. N1). The development of flexural strength from 7 to 28 days was higher for N1, with a 79% increase, while N2 and N3 showed 68% and 59% increases, respectively. The situation reversed from 28 to 91 days, when the growth of N3, N2 and N1 was 71%, 48% and

37%, respectively. For mixes with Na_2SiO_3, flexural and compressive strengths increased with a higher content of the activator, which indicates that the ratio between the amount of NaOH and precursor may not have been enough to promote dissolution of SiO_2 and Al_2O_3 (Hamidi et al., 2016). NS2 showed a decrease in strength after the 7th day, while the rest practically stabilized after the 28th day.
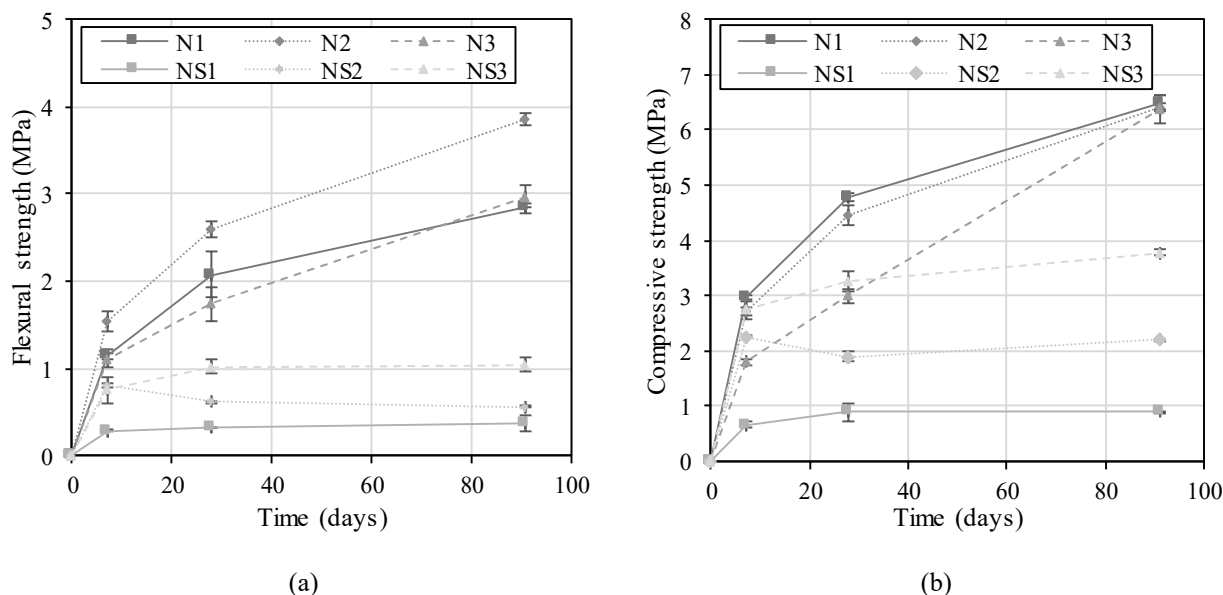

(a)   (b)

Figure 7 - Variation of flexural (a) and compressive strength (b) over time

The specimens were completely carbonated after 28 days inside the carbonation chamber, which prevented any conclusions concerning the diffusion of CO_2. Before being introduced into the chamber, their curing regimen was the same as that of the other specimens up to 28 days and thus this test allows understanding the effect of carbonation on the flexural and compressive strengths (Figure 8 and Figure 9, respectively).

From 28 to 56 days, all mixes showed increased strength. N3 and NS3 mixes exhibited the best results and were the ones with higher concentrations of NaOH. Almost all carbonated specimens exhibited strength loss from 56 to 119 days. $CaCO_3$ and amorphous SiO_2 gel are formed in the C_3S carbonation process, which bonds together to form a dense matrix, significantly increasing the material's strength (Li et al., 2018). However, this process generates tension around unreacted particles in carbonated areas, causing micro-cracking, due to carbonation-induced shrinkage, resulting in strength loss after a long exposure to CO_2 (Bernal et al., 2013).
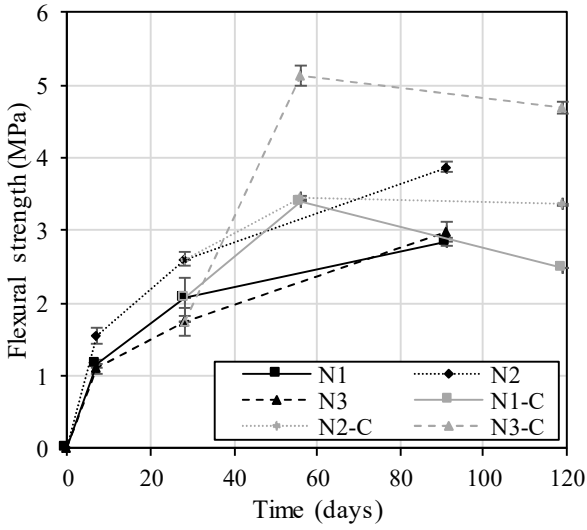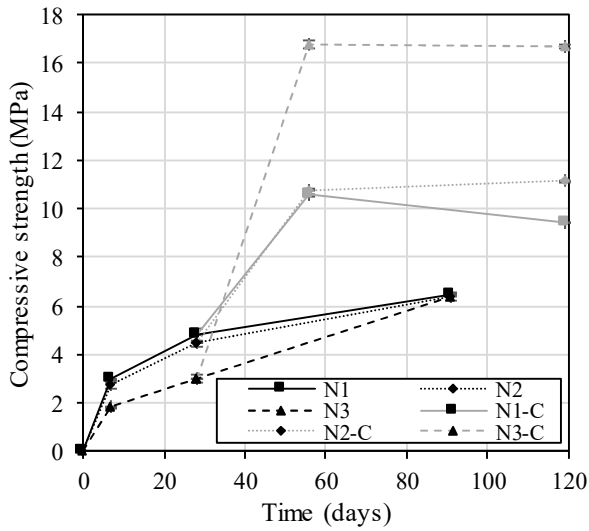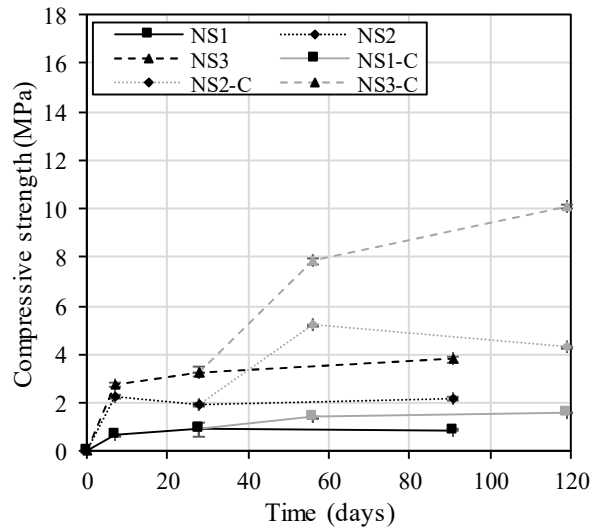
(a)
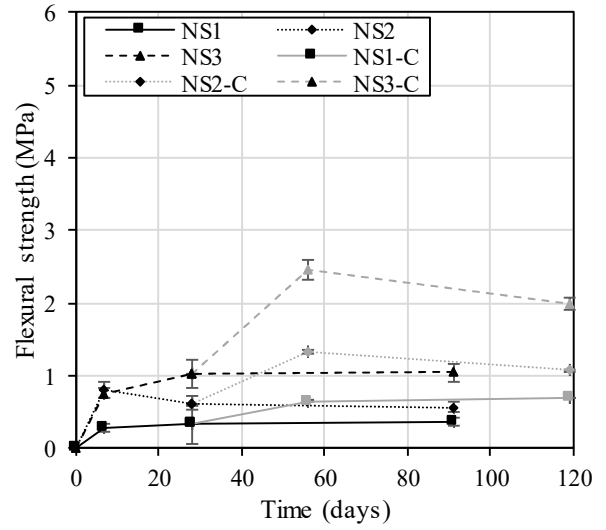
(b)

Figure 8 - Variation of flexural strength of carbonated samples of families with (a) NaOH and (b) Na_2SiO_3 over time

(a)

(b)

Figure 9 - Variation of compressive strength of carbonated samples of families with (a) NaOH and (b) Na_2SiO_3 over time

The results of the shrinkage test are presented in Figure 10. N1 showed the largest dimensional variation. This was expected due to the poor results in the dynamic modulus of elasticity test (Table 4) inferring a less rigid matrix. Comparing N2 and N3, despite the similar values of modulus of elasticity, N3 exhibited less shrinkage, probably due to the initial expansion of the material.

Concerning the mortars with Na_2SiO_3, higher activator content led to higher microstrain. Contrary to expectations, this property did not correlate with the ultrasonic pulse velocity or modulus of elasticity. In the production of NS3 specimens, due to loss of material after mixing because of the ongoing expansive reactions of H_2 gas release, a lightweight and porous material was obtained, leading to greater dimensional variation.
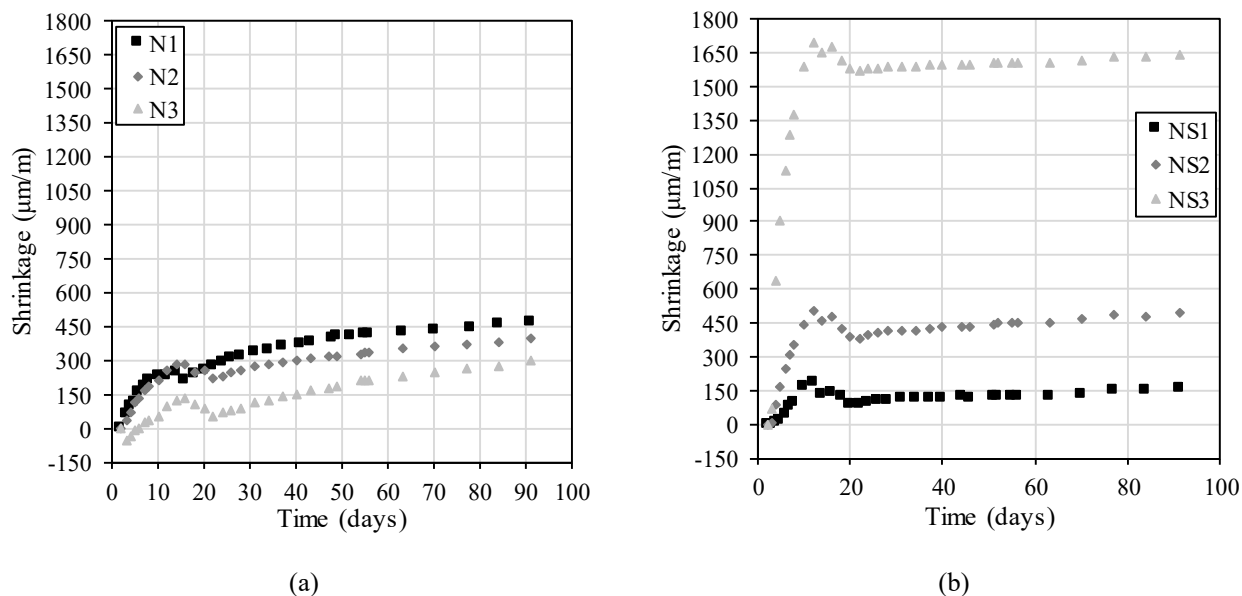
(a)   (b)

Figure 10 - Dimensional variation of families with (a) NaOH and (b) Na$_2$SiO$_3$

Table 4 - Dynamic modulus of elasticity and coefficient of water absorption by capillarity

Mix	Dynamic modulus of elasticity						Coefficient of water absorption by capillarity	
	7-day		28-day		91-day		10 - 90 min	
	$\bar{x}$ (GPa)	s (GPa)	$\bar{x}$ (GPa)	s (GPa)	$\bar{x}$ (GPa)	s (GPa)	$\bar{x}$ (kg/(m^2.min$^{0.5}$))	s (kg/(m^2.min$^{0.5}$))
N1	4.96	0.34	6.99	0.33	8.06	0.63	0.268	0.022
N2	5.72	0.26	8.11	0.37	10.90	0.70	0.208	0.016
N3	5.02	0.27	7.50	0.14	10.54	0.51	0.107	0.018
NS1	1.33	0.09	1.75	0.02	1.79	0.02	0.337	0.022
NS2	1.78	0.09	2.25	0.09	1.90	0.21	0.278	0.031
NS3	1.76	0.06	2.73	0.06	3.38	0.19	0.117	0.017

The results of the water absorption by capillary action test (Table 4) show that, for all NaOH and Na$_2$SiO$_3$ mixes, the coefficient decreased with increasing AA concentration. Huseien *et al.* (2018) also showed a decrease in water absorption with increasing NaOH concentration due to greater dissolution of reactive material thereby leading to a more homogeneous and denser microstructure. A higher coefficient was observed in Na$_2$SiO$_3$-based mixes. Based on visual assessment and previous tests, it would be expected for these mortars to present higher coefficients. One possible explanation for this reduced mass gain over time could be the presence of pores with large diameters, thereby reducing the surface tension consequently decreasing the water absorbed by capillarity. Also, the mass gain was hindered by the mortars' poor physical stability, causing leaching. This led to brown-coloured test water, probably due to leached ferrous compounds, which, apart from not dissolving in an alkaline environment, can form bonds with Al in a spinel system or with

19

iron-rich glasses, decreasing the available amount of Al and Si for the polymerization reactions (Chen-Tan et al., 2009). The precipitated material, resulting from the evaporation of water from each test, was analysed by XRD. The water from mortars with NaOH produced thermonatrite ($Na_2CO_3 \cdot H_2O$ - ICDD # 001-1015) and halite (NaCl - ICDD # 001-0994), whereas the water from Na_2SiO_3-based mortars produced thermonatrite ($Na_2CO_3 \cdot H_2O$ - ICDD # 001-1015), halite (NaCl - ICDD # 001-0994), natrite (Na_2CO_3 - ICDD # 37-0451), trona ($Na_3H(CO_3)_2 \cdot 2H_2O$ - ICDD # 029-1447) and nahcolite ($NaHCO_3$ - ICDD # 01-0909).

3.4 Compositional analysis of pastes

Two pastes with NaOH (N2 - cured in the dry chamber; N2-C - cured in the carbonation chamber) and one paste with Na_2SiO_3 (NS2 - cured in the dry chamber) were submitted to an XRD analysis (Figure 11). The XRD of N2 demonstrated the occurrence of polymerization reactions corroborated by the presence of hydrated sodium alumi-nosilicate ($Na_6[AlSiO_4]_6 \cdot 4H_2O$). Hydrated calcium aluminates ($Ca_4Al_2O_7 \cdot 19H_2O$), hydrated sodium carbonate ($Na_2CO_3 \cdot 7H_2O$) were also identified, as well as crystalline SiO_2, which came from the precursor and is present in all samples. The carbonated paste (N2-C) contained, besides SiO_2, calcium silicate hydrate ($Ca_{1.5}SiO_{3.5}$ xH_2O) or C-S-H, aragonite ($CaCO_3$) and nahcolite ($NaHCO_3$). The two latter products are normal in carbonated AAM, but the formation of nahcolite ($NaHCO_3$) is favoured under conditions of accelerated carbonation (Pouhet and Cyr, 2016). The presence of $CaCO_3$ and amorphous SiO_2 through the carbonation process of C_3S generates a potentially stronger cohesive force than C-S-H gel (Li et al., 2018), thereby explain the considerable strength development of carbonated mixes. The result of the NS2 XRD test identified quartz, calcite ($CaCO_3$), pirssonite ($Na_2Ca(CO_3)_2 \cdot 2(H_2O)$) and also precipitated sodium hydroxide (NaOH).
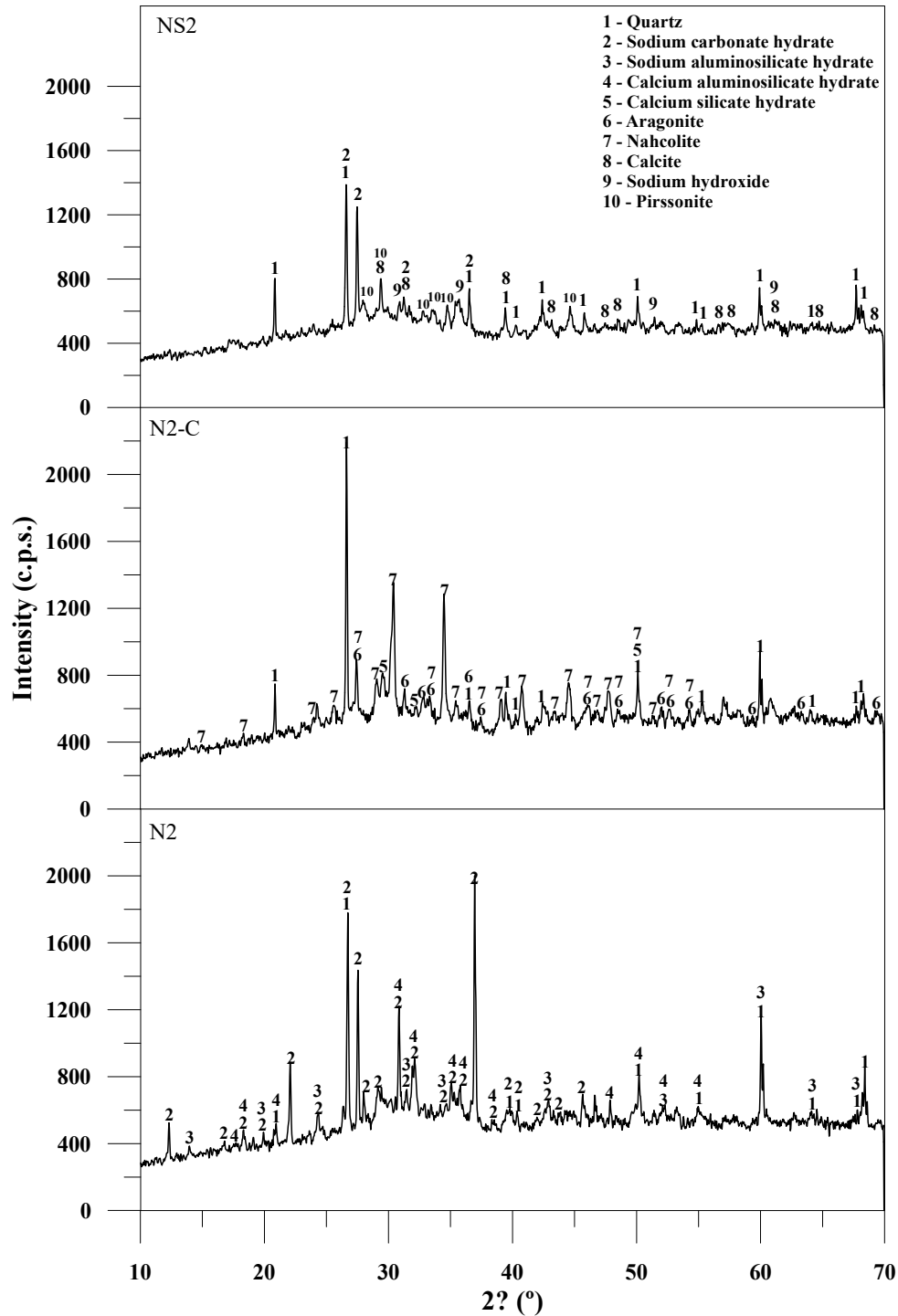
Figure 11 - XRD analysis of (un)carbonated pastes with NaOH and Na₂SiO₃

4 Conclusions

An experimental investigation on the influence of NaOH and Na_2SiO_3, as alkali activators in the production of mortars with MIBA as a precursor, was carried out. Despite the low amount of Al_2O_3 in MIBA, its chemical composition resembles that of class C FA; however, the former contains a lower amount of amorphous material (mostly from discarded waste glass), leading to a material with relatively low pozzolanicity

21

and thus poor reactivity in an alkaline medium. Processed MIBA contains a notable amount of ferrous metals due to the ineffective electromagnetic separation stage applied at the treatment facility. This treatment process could be improved, wherein potentially higher revenue would be obtained from selling the removed metal and less contaminated MIBA would be produced. However, due to the inherent little effectiveness of the eddy current separation stage for non-ferrous metals, metallic Al is likely to be present in every batch of MIBA. This component will react with the OH^- present in the alkaline solution causing the formation of H_2 gas, which becomes entrapped in the fresh mix. After the thermal curing process, which also potentiates this reaction, all samples showed expansion, despite the resting period to allow the release of H_2 gas. Naturally, the higher porosity derived from this expansion, which can also occur in conventional concrete, allied with the relatively lower reactivity of MIBA in comparison with FA, led to a considerable decline in mechanical and durability related performances.

Enhanced performance was observed in mixes using NaOH as the activator in comparison with those made with Na_2SiO_3. Despite the same amount of activator for both mixes, the improved performance by the former may have been due to the higher amount of OH^- ions in the aqueous solution, leading to a high pH environment, thereby potentiating dissolution of the reactive aluminosilicates. Therefore, contrary to that typically observed in AAM with other precursors, the presence of Na_2SiO_3 may hinder the mechanical performance and should be minimized in MIBA-based AAM.

All AAM samples exhibited a fast decline in pH levels thus affecting the material's resistance to carbonation. However, these specimens also showed considerably enhanced mechanical performance when subjected to accelerated carbonation. The presence of CO_2 led to a decalcification of some phases and decrease of sodium-based ones, consequently forming calcium carbonate polymorphs (mostly aragonite) and the presence of amorphous SiO_2 gel, which significantly increased strength. From a practical application perspective, despite the evident shortcomings of the material, further research will provide additional insight on how to best valorize MIBA as partial/complete replacement of mineral additions that are phasing out. Furthermore, not only do these materials present a notable carbon sequestration ability, which can be interesting in capturing the CO_2 from redirected flue gases from industries, but they also present a significant performance

enhancement with continuous carbonation to a point that the aforementioned shortcomings are eliminated.

Acknowledgements

Data availability

The raw/processed data required to reproduce these findings cannot be shared at this time as the data is part of an ongoing study.

References

Ascensão, G., Marchi, M., Segata, M., Faleschini, F., Pontikes, Y., 2020. Reaction kinetics and structural analysis of alkali activated Fe-Si-Ca rich materials. J. Clean. Prod. 246, 119065 https://doi.org/10.1016/j.jclepro.2019.119065.

ASTM-C618, 2019. Standard specification for coal fly ash and raw or calcined natural pozzolan for use in concrete. American Society for Testing and Materials, West Conshohocken, Pennsylvania, USA, 5 p.

ASTM-E1876, 2015. Standard test method for dynamic Young's modulus, shear modulus, and Poisson's ratio by impulse excitation of vibration. American Society for Testing and Materials, West Conshohocken, Pennsylvania, USA, 17 p.

Benhelal, E., Zahedi, G., Shamsaei, E., Bahadori, A., 2013. Global strategies and potentials to curb CO2 emissions in cement industry. J. Clean. Prod. 51 (Supplement C), 142-161. https://doi.org/10.1016/j.jclepro.2012.10.049.

Bernal, S.A., Provis, J.L., Walkley, B., San Nicolas, R., Gehman, J.D., Brice, D.G., Kilcullen, A.R., Duxson, P., van Deventer, J.S.J., 2013. Gel nanostructure in alkali-activated binders based on slag and fly ash, and effects of accelerated carbonation. Cem. Concr. Res. 53, 127-144. https://doi.org/10.1016/j.cemconres.2013.06.007.

Chen-Tan, N.W., Van Riessen, A., LY, C.V., Southam, D.C., 2009. Determining the reactivity of a fly ash for production of geopolymer. J. Am. Ceram. Soc. 92(4), 881-887. https://doi.org/10.1111/j.1551-2916.2009.02948.x.

Chen, Z., Liu, Y., Zhu, W., Yang, E.H., 2016. Incinerator bottom ash (IBA) aerated geopolymer. Constr. Build. Mater. 112, 1025-1031. https://doi.org/10.1016/j.conbuildmat.2016.02.164.

Cyr, M., Pouhet, R., 2016. Carbonation in the pore solution of metakaolin-based geopolymer. Cem. Concr. Res. 88, 227-235. https://doi.org/10.1016/j.cemconres.2016.05.008.

Davidovits, J., 1994. Properties of geopolymer cements, Proceedings of the First International Conference on Alkaline Cements and Concretes. Scientific Research Institute on Binders and Materials, Kiev State Technical University, Kiev, Ukraine, pp. 131-149.

Dhir, R.K., De Brito, J., Lynn, C.J., Silva, R.V., 2018. Sustainable construction materials: Municipal incinerator bottom ashes, first ed. Woodhead Publishing, Duxford, UK.

EN-450-1, 2012. Fly ash for concrete. Definition, specifications and conformity criteria. Comité Européen de Normalisation (CEN), Brussels, Belgium, 34 p.

EN-1015-1, 1999. Methods of test for mortar for masonry - Part 1: Determination of particle size distribution (by sieve analysis). Comité Européen de Normalisation (CEN), Brussels, Belgium, 8 p.

EN-1015-2, 1999. Methods of test for mortar for masonry - Part 2: Bulk sampling of mortars and preparation of test mortars. Comité Européen de Normalisation (CEN), Brussels, Belgium, 8 p.

EN-1015-3, 1999. Methods of test for mortar for masonry - Part 3: Determination of consistence of fresh mortar (by flow table). Comité Européen de Normalisation (CEN), Brussels, Belgium, 10p.

EN-1015-6, 1999. Methods of test for mortar for masonry - Part 6: Determination of bulk density of fresh mortar. Comité Européen de Normalisation (CEN), Brussels, Belgium, 8 p.

EN-1015-11, 1999. Methods of test for mortar for masonry - Part 11: Determination of flexural and compressive strength of hardened mortar. Comité Européen de Normalisation (CEN), Brussels, Belgium, 12 p.

EN-1015-13, 1993. Methods of test for mortar for masonry - Part 13: Determination of dimensional stability of hardened mortars. Comité Européen de Normalisation (CEN), Brussels, Belgium, 20 p.

EN-1015-18, 2002. Methods of test for mortar for masonry - Part 18: Determination of water absorption coefficient due to capillary action of hardened mortar. Comité Européen de Normalisation (CEN), Brussels, Belgium, 12 p.

EN-1097-3, 1998. Tests for mechanical and physical properties of aggregates - Part 3: Determination of loose bulk density and voids. Comité Européen de Normalisation (CEN), Brussels, Belgium, 10 p.

EN-1097-5, 2008. Tests for mechanical and physical properties of aggregates - Part 5: Determination of the water content by drying in a ventilated oven. Comité Européen de Normalisation (CEN), Brussels, Belgium, 54 p.

Ferraz, E., Andrejkovičová, S., Hajjaji, W., Velosa, A.L., Silva, A.S., Rocha, F., 2015. Pozzolanic activity of metakaolins by the French Standard of the modified Chapelle Test: A direct methodology. Acta Geodynamicaet Geometerialia Aspects 12, 289-298. https://doi.org/10.13168/AGG.2015.0026.

Golek, L., 2019. Glass powder and high-calcium fly ash based binders - Long term examinations. J. Clean. Prod. 220, 493-506. https://doi.org/10.1016/j.jclepro.2019.02.095.

Hamidi, R.M., Man, Z., Azizli, K.A., 2016. Concentration of NaOH and the Effect on the Properties of Fly Ash Based Geopolymer. Procedia Engineer. 148, 189-193. https://doi.org/10.1016/j.proeng.2016.06.568.

Huang, G., Ji, Y., Li, J., Zhang, L., Liu, X., Liu, B., 2019. Effect of activated silica on polymerization mechanism and strength development of MSWI bottom ash alkali-activated mortars. Constr. Build. Mater. 201, 90-99. https://doi.org/10.1016/j.conbuildmat.2018.12.125.

Huang, G., Ji, Y., Zhang, L., Li, J., Hou, Z., 2018. The influence of curing methods on the strength of MSWI bottom ash-based alkali-activated mortars: The role of leaching of OH^- and free alkali. Constr. Build. Mater. 186, 978-985. https://doi.org/10.1016/j.conbuildmat.2018.07.224.

Huseien, G.F., Ismail, M., Khalid, N.H.A., Hussin, M.W., Mirza, J., 2018. Compressive strength and microstructure of assorted wastes incorporated geopolymer mortars: Effect of solution molarity. Alexandria Engineering Journal 57(4), 3375-3386. https://doi.org/10.1016/j.aej.2018.07.011.

Kim, Y., Kang, S., 2014. Characterization of geopolymer made of municipal solid waste incineration ash slag. J. Korean Cryst. Growth Cryst. Technol. 24(1), 15-20. https://doi.org/10.6111/jkcgct.2014.24.1.015.

Kurda, R., Silva, R.V., de Brito, J., 2020. Incorporation of alkali-activated municipal solid waste incinerator bottom ash in mortar and concrete: A critical review. Materials 13(15), 3428. https://doi.org/10.3390/ma13153428.

Li, Z., He, Z., Shao, Y., 2018. Early age carbonation heat and products of tricalcium silicate paste subject to carbon dioxide curing. Materials 11(5), 730. https://doi.org/10.3390/ma11050730.

LNEC-E391, 1993. Concrete: determination of carbonation resistance (in Portuguese). National Laboratory in Civil Engineering (LNEC - Laboratório Nacional de Engenharia Civil) Lisbon, Portugal, 2 p.

Luukkonen, T., Abdollahnejad, Z., Yliniemi, J., Kinnunen, P., Illikainen, M., 2018. One-part alkali-activated materials: A review. Cem. Concr. Res. 103, 21-34. https://doi.org/10.1016/j.cemconres.2017.10.001.

NBR-15895, 2010. Materiais pozolânicos - Determinação do teor de hidróxido de cálcio fixado - Método de Chapelle modificado. Brazilian Association for Technical Norms (Associação Brasileira de Normas Técnicas - ABNT), Rio de Janeiro, Brasil, 10 p.

Nepomuceno, M., Oliveira, L., Lopes, S.M.R., 2012. Methodology for mix design of the mortar phase of self-compacting concrete using different mineral additions in binary blends of powders. Constr. Build. Mater. 26(1), 317-326. http://dx.doi.org/10.1016/j.conbuildmat.2011.06.0kou27.

Olivia, M., Nikraz, H., 2012. Properties of fly ash geopolymer concrete designed by Taguchi method. Mater. Des. 36, 191-198. https://doi.org/10.1016/j.matdes.2011.10.036.

Ozturk, M., Bankir, M.B., Bolukbasi, O.S., Sevim, U.K., 2019. Alkali activation of electric arc furnace slag: Mechanical properties and micro analyzes. J. Build. Eng. 21, 97-105. https://doi.org/10.1016/j.jobe.2018.10.005.

Palacios, M., Banfill, P.F., Puertas, F., 2008. Rheology and setting of alkali-activated slag pastes and mortars: effect of organic admixture. ACI Mater. J. 105(2), 140. https://doi.org/10.14359/19754.

Provis, J.L., van Deventer, J.S.J., 2014. Alkali Activated Materials - State-of-the-Art Report, RILEM TC 224-AAM. first ed. Springer, Rotterdam, The Netherlands.

Raverdy, M., Brivot, F., Paillere, A.M., Dron, R., 1980. Appreciation of pozzolanic reactivity of secondary components (in French), 7eme Congres International de la Chimie Des Ciments Paris France.

Schalenbach, M., Zeradjanin, A., Kasian, O., Cherevko, S., Mayrhofer, K., 2018. A Perspective on Low-Temperature Water Electrolysis - Challenges in Alkaline and Acidic Technology. International Journal of Electrochemical Science 13, 1173-1226. https://doi.org/10.20964/2018.02.26.

Silva, R.V., de Brito, J., Lynn, C.J., Dhir, R.K., 2017. Use of municipal solid waste incineration bottom ashes in alkali-activated materials, ceramics and granular applications: A review. Waste Manage. 68, 207-220. https://doi.org/10.1016/j.wasman.2017.06.043.

Tang, P., 2017. Municipal solid waste incineration (MSWI) bottom ash - from waste to value. PhD Thesis, Technische Universiteit Eindhoven, Eindhoven, Germany, 197 p.

Wongsa, A., Boonserm, K., Waisurasingha, C., Sata, V., Chindaprasirt, P., 2017. Use of municipal solid waste incinerator (MSWI) bottom ash in high calcium fly ash geopolymer matrix. J. Clean. Prod. 148, 49-59. https://doi.org/10.1016/j.jclepro.2017.01.147.

Yang, K.H., Song, J.K., Song, K.I., 2013. Assessment of CO_2 reduction of alkali-activated concrete. J. Clean. Prod. 39, 265-272. http://dx.doi.org/10.1016/j.jclepro.2012.08.001.

Zhu, W., Chen, X., Struble, L., Yang, E., 2018. Characterization of calcium-containing phases in alkali-activated municipal solid waste incineration bottom ash binder through chemical extraction and deconvoluted Fourier transform infrared spectra. J. Clean. Prod. 192, 782-789. https://doi.org/10.1016/j.jclepro.2018.05.049.

Zhu, W.P., Chen, X., Zhao, A.Q., Struble, L.J., Yang, E.H., 2019. Synthesis of high strength binders from alkali activation of glass materials from municipal solid waste incineration bottom ash. J. Clean. Prod. 212, 261-269. https://doi.org/10.1016/j.jclepro.2018.11.295

List of Tables

List of Figures